Continuum quasiparticle random phase approximation and the time-dependent Hartree-Fock-Bogoliubov approach

E. Khan,[1] N. Sandulescu,[2,3,4] M. Grasso,[1] and Nguyen Van Giai[1]
[1]*Institut de Physique Nucléaire, IN_2P_3-CNRS, F-91406 Orsay, France*
[2]*Institute for Physics and Nuclear Engineering, P.O. Box MG-6, 76900 Bucharest, Romania*
[3]*Research Center for Nuclear Physics, Osaka University, 567-0047 Osaka, Japan*
[4]*Royal Institute of Technology, SCFAB, SE-10691 Stockholm, Sweden*
(Received 21 March 2002; published 6 August 2002)

Quadrupole excitations of neutron-rich nuclei are analyzed by using the linear response method in the quasiparticle random phase approximation (QRPA). The QRPA response is derived starting from the time-dependent Hartree-Fock-Bogoliubov (HFB) equations. The residual interaction between the quasiparticles is determined consistently from the two-body force used in the HFB equations, and the continuum coupling is treated exactly. Calculations are done for the neutron-rich oxygen isotopes. It is found that pairing correlations affect the low-lying states, and that a full treatment of the continuum can change the structure of the states in the giant resonance region.

DOI: 10.1103/PhysRevC.66.024309 PACS number(s): 24.30.Cz, 21.60.Jz, 27.60.+j

I. INTRODUCTION

The collective excitations of atomic nuclei in the presence of pairing correlations is usually described in the quasiparticle random phase approximation (QRPA) [1]. Although the QRPA was applied to nuclear physics more than 40 years ago [2–4], recently there is a renewed interest on its grounds, generated mainly by the studies of unstable nuclei close to the drip line. In these nuclei characterized by a small nucleon separation energy, the excited states are strongly influenced by the coupling with the quasiparticle (qp) continuum configurations. Among the configurations of particular interest are the two-qp states in which one or both quasiparticles are in the continuum. In order to describe such excited states within QRPA one needs a proper treatment of the continuum coupling, which is missing in the usual QRPA calculations based on a discrete qp spectrum.

In nuclei close to the drip lines one expects also a strong connection between the excitations of the system and the properties of the ground state, which may present such specificities as neutron skins. Therefore, in addition to the qp spectrum, the residual interaction used in QRPA should be determined from the same two-body force as it is done in the self-consistent continuum RPA calculations [5–7].

In the past years several attempts [8–10] have been made to describe consistently both the pairing correlations and the continuum coupling within QRPA. Thus, in Ref. [9] a QRPA approach was recently developed in which the effect of the continuum is calculated exactly for the particle-hole excitations whereas in the particle-particle channel the active space is limited to the bound states close to the Fermi level.

A continuum qp linear response approach in which the continuum is included also in the particle-particle channel was studied in Ref. [10], but in the calculations the ground state mean field is fixed independently of the residual interaction.

In this paper we present the first continuum QRPA calculations with the single-particle spectrum and the residual interaction determined from the same effective two-body force. The ground state is calculated using the continuum Hartree-Fock-Bogoliubov (HFB) approach [11] with the mean field and the pairing field described by a Skyrme interaction and a density dependent delta force, respectively. Based on the same HFB energy functional we derive the QRPA response function in coordinate space. The QRPA response is constructed by using real energy solutions for the continuum HFB spectrum. The calculations are done for the neutron-rich oxygen isotopes.

In Sec. II we present the continuum QRPA formalism, we specialize the corresponding equations to systems with spherical symmetry and we discuss the energy-weighted sum rule in QRPA. The application of the present theory to neutron-rich oxygen isotopes is done in Sec. III. Section IV contains the concluding remarks.

II. FORMALISM

A. Derivation of the generalized Bethe-Salpeter equation

The coordinate space formalism is naturally adapted to treat properly the coupling to the continuum states. In this section we derive the QRPA equations in coordinate space as the small amplitude limit of the perturbed time-dependent HFB equations. We start from the time-dependent HFB (TDHFB) equations [1],

$$i\hbar \frac{\partial \mathcal{R}}{\partial t} = [\mathcal{H}(t) + \mathcal{F}(t), \mathcal{R}(t)], \tag{2.1}$$

where $\mathcal{R}$ and $\mathcal{H}$ are the time-dependent generalized density and HFB Hamiltonian. The external periodic field $\mathcal{F}$ is given by

$$\mathcal{F} = F e^{-i\omega t} + \text{H.c.}, \tag{2.2}$$

where F includes both particle-hole and two-particle transfer operators,

$$F=\sum_{ij} F_{ij}^{11}c_i^\dagger c_j+\sum_{ij}\left(F_{ij}^{12}c_i^\dagger c_j^\dagger+F_{ij}^{21}c_i c_j\right) \tag{2.3}$$

and $c_i^\dagger$, c_i are the particle creation and annihilation operators, respectively. Assuming that the external field induces small oscillations around the stationary solution of the HFB equations,

$$\mathcal{R}(t)=\mathcal{R}^0+\mathcal{R}'e^{-i\omega t}+\text{H.c.}, \tag{2.4}$$

$$\mathcal{H}(t)=\mathcal{H}^0+\mathcal{H}'e^{-i\omega t}+\text{H.c.} \tag{2.5}$$

the TDHFB equation (2.1) becomes

$$\hbar\omega\mathcal{R}'=[\mathcal{H}',\mathcal{R}^0]+[\mathcal{H}^0,\mathcal{R}']+[F,\mathcal{R}^0]. \tag{2.6}$$

The generalized density variation has the form

$$\mathcal{R}'_{ij}=\begin{pmatrix}\rho'_{ij} & \kappa'_{ij}\\ \overline{\kappa'_{ij}} & -\rho'_{ji}\end{pmatrix}, \tag{2.7}$$

where $\rho'_{ij}=\langle 0|c_j^\dagger c_i|'\rangle$ is the variation of the particle density, $\kappa'_{ij}=\langle 0|c_j c_i|'\rangle$ and $\overline{\kappa'_{ij}}=\langle 0|c_j^\dagger c_i^\dagger|'\rangle$ are the fluctuations of the pairing tensor associated with the pairing vibrations and $|'\rangle$ denotes the change of the ground state wave function $|0\rangle$ due to the external field. Instead of the variation of one quantity in RPA (ρ'), we now have to know the variations of three independent quantities in QRPA, namely, ρ', κ', and $\overline{\kappa'}$.

It is convenient to solve Eq. (2.6) in the qp representation in which both $\mathcal{H}^0$ and $\mathcal{R}^0$ are diagonal [1]. We have now to express all quantities of Eq. (2.6) in this representation. The matrix $\mathcal{R}'$ becomes off-diagonal because of the TDHFB condition $\mathcal{R}'^2=\mathcal{R}'$ imposed on Eq. (2.4),

$$\tilde{\mathcal{R}}'_{ij}=\begin{pmatrix}0 & \tilde{\mathcal{R}}'^{12}_{ij}\\ \tilde{\mathcal{R}}'^{21}_{ij} & 0\end{pmatrix}=\begin{pmatrix}0 & \langle 0|\beta_j\beta_i|'\rangle\\ \langle 0|\beta_j^\dagger\beta_i^\dagger|'\rangle & 0\end{pmatrix}, \tag{2.8}$$

where $\beta_i^\dagger$, β_i are, respectively, the qp creation and annihilation operators of an HFB state i with energy E_i. Consequently, Eq. (2.6) gives

$$\tilde{\mathcal{R}}'^{12}_{ij}=\frac{\tilde{\mathcal{H}}'^{12}_{ij}+\tilde{F}^{12}_{ij}}{\hbar\omega-(E_i+E_j)}, \tag{2.9}$$

$$\tilde{\mathcal{R}}'^{21}_{ij}=-\frac{\tilde{\mathcal{H}}'^{21}_{ij}+\tilde{F}^{21}_{ij}}{\hbar\omega+(E_i+E_j)}. \tag{2.10}$$

Here, $\tilde{\mathcal{H}}'$ and $\tilde{F}$ stand for $\mathcal{H}'$ and F in the qp representation.

We now proceed to calculate $\tilde{\mathcal{H}}'^{12}_{ij}$ and $\tilde{\mathcal{H}}'^{21}_{ij}$. The variations of the particle and pairing densities in coordinate representation are defined by

$$\rho'(\mathbf{r}\sigma)=\langle 0|\psi^\dagger(\mathbf{r}\sigma)\psi(\mathbf{r}\sigma)|'\rangle, \tag{2.11}$$

$$\kappa'(\mathbf{r}\sigma)=\langle 0|\psi(\mathbf{r}\overline{\sigma})\psi(\mathbf{r}\sigma)|'\rangle, \tag{2.12}$$

$$\overline{\kappa'}(\mathbf{r}\sigma)=\langle 0|\psi^\dagger(\mathbf{r}\sigma)\psi^\dagger(\mathbf{r}\overline{\sigma})|'\rangle, \tag{2.13}$$

where $\psi^\dagger(\mathbf{r}\sigma)$ is the particle creation operator in coordinate space and $\psi^\dagger(\mathbf{r}\overline{\sigma})=-2\sigma\psi^\dagger(\mathbf{r}-\sigma)$ is its time reversed counterpart. The relation between the $\psi^\dagger,\psi$ and $\beta^\dagger,\beta$ operators is

$$\psi^\dagger(\mathbf{r}\sigma)=\sum_k U_k(\mathbf{r}\sigma)\beta_k+V_k^*(\mathbf{r}\sigma)\beta_k^\dagger, \tag{2.14}$$

where U_k and V_k are the two components of the HFB wave function of the qp state with energy E_k.

Introducing Eq. (2.14) and its Hermitian conjugate into Eqs. (2.11)–(2.13) one gets with the help of Eq. (2.8),

$$\rho'_\alpha(\mathbf{r}\sigma)=\sum_{ij}\mathcal{U}_{ij}^{\alpha 1}(\mathbf{r}\sigma)\tilde{\mathcal{R}}'^{12}_{ij}+\mathcal{U}_{ij}^{\alpha 2}(\mathbf{r}\sigma)\tilde{\mathcal{R}}'^{21}_{ij},\quad \alpha=1,2,3, \tag{2.15}$$

where we have introduced the following notation for the density variations:

$$\boldsymbol{\rho}'=\begin{pmatrix}\rho'_1\\ \rho'_2\\ \rho'_3\end{pmatrix}=\begin{pmatrix}\rho'\\ \kappa'\\ \overline{\kappa'}\end{pmatrix} \tag{2.16}$$

and the 3×2 matrices $\mathcal{U}_{ij}$ are defined by

$$\mathcal{U}_{ij}(\mathbf{r}\sigma)=\begin{pmatrix}U_i(\mathbf{r}\sigma)V_j(\mathbf{r}\sigma) & U_j^*(\mathbf{r}\sigma)V_i^*(\mathbf{r}\sigma)\\ U_i(\mathbf{r}\sigma)U_j(\mathbf{r}\overline{\sigma}) & V_i^*(\mathbf{r}\sigma)V_j^*(\mathbf{r}\overline{\sigma})\\ -V_i(\mathbf{r}\sigma)V_j(\mathbf{r}\overline{\sigma}) & -U_i^*(\mathbf{r}\sigma)U_j^*(\mathbf{r}\overline{\sigma})\end{pmatrix}. \tag{2.17}$$

Here, we have used the same notation as introduced before for the time reversed particle operators, i.e., $f(\mathbf{r}\overline{\sigma})=-2\sigma f(\mathbf{r}-\sigma)$.

Next, we must calculate the variation $\tilde{\mathcal{H}}'$ of the HFB Hamiltonian in the qp representation. This is obtained from the corresponding quantity in coordinate representation through the transformation [1],

$$\tilde{\mathcal{H}}'=W^\dagger\mathcal{H}'W, \tag{2.18}$$

where the matrix W is defined by

$$W=\begin{pmatrix}U & V^*\\ V & U^*\end{pmatrix}. \tag{2.19}$$

One thus gets

$$\tilde{\mathcal{H}}'^{12}_{ij}=\int d\mathbf{r}\sum_\sigma \overline{\mathcal{U}}_{ij}^{*11}(\mathbf{r}\sigma)\mathcal{H}'^{11}(\mathbf{r})-\overline{\mathcal{U}}_{ij}^{\dagger 21}(\mathbf{r}\sigma)\mathcal{H}'^{12}(\mathbf{r})$$
$$-\overline{\mathcal{U}}_{ij}^{\dagger 31}(\mathbf{r}\sigma)\mathcal{H}'^{21}(\mathbf{r}), \tag{2.20}$$

$$\tilde{\mathcal{H}}'^{21}_{ij} = \int d\mathbf{r} \sum_{\sigma} \bar{\mathcal{U}}^{*12}_{ij}(\mathbf{r}\sigma)\mathcal{H}'^{11}(\mathbf{r}) - \bar{\mathcal{U}}^{\dagger 22}_{ij}(\mathbf{r}\sigma)\mathcal{H}'^{12}(\mathbf{r}) - \bar{\mathcal{U}}^{\dagger 32}_{ij}(\mathbf{r}\sigma)\mathcal{H}'^{21}(\mathbf{r}), \tag{2.21}$$

where $\bar{\mathcal{U}}_{ij} = \mathcal{U}_{ij} - \mathcal{U}_{ji}$. This antisymmetric combination appears by taking into account the relation $\mathcal{H}'^{22}_{ij} = -\mathcal{H}'^{11}_{ji}$ [1]. Similar equations hold for the matrix elements of the external field (2.3).

In coordinate representation the variation of the HFB Hamiltonian is expressed in terms of the second derivatives of the HFB energy functional $\mathcal{E}[\rho, \kappa, \bar{\kappa}]$ with respect to the densities. Thus, in our matrix notation we can write (see Appendix)

$$\boldsymbol{\mathcal{H}}' = \begin{pmatrix} \mathcal{H}'^{11} \\ \mathcal{H}'^{12} \\ \mathcal{H}'^{21} \end{pmatrix} = \mathbf{V}\boldsymbol{\rho}', \tag{2.22}$$

where $\mathbf{V}$ is the residual interaction matrix, namely,

$$\mathbf{V}^{\alpha\beta}(\mathbf{r}\sigma, \mathbf{r}'\sigma') = \frac{\partial^2 \mathcal{E}}{\partial \rho_{\beta}(\mathbf{r}'\sigma')\partial \rho_{\bar{\alpha}}(\mathbf{r}\sigma)}, \quad \alpha, \beta = 1,2,3. \tag{2.23}$$

Here, the notation $\bar{\alpha}$ means that whenever α is 2 or 3 then $\bar{\alpha}$ is 3 or 2.

It should be noted that in the three dimensional space, the first dimension represents the particle-hole (ph) subspace, the second the particle-particle (pp) one, and the third the hole-hole (hh) one. This is due to the definitions (2.11)–(2.13).

Using Eqs. (2.9), (2.10), (2.15), and (2.20)–(2.22), we finally land on the coupled equations

$$\boldsymbol{\rho}' = \mathbf{G}_0\mathbf{V}\boldsymbol{\rho}' + \mathbf{G}_0\mathbf{F}, \tag{2.24}$$

where $\mathbf{F}$ is the three dimensional column vector

$$\mathbf{F} = \begin{pmatrix} F^{11} \\ F^{12} \\ F^{21} \end{pmatrix} \tag{2.25}$$

and $\mathbf{G}_0$ is the unperturbed Green function defined by

$$\mathbf{G}_0^{\alpha\beta}(\mathbf{r}\sigma, \mathbf{r}'\sigma'; \omega) = \sum_{ij} \frac{\mathcal{U}^{\alpha 1}_{ij}(\mathbf{r}\sigma)\bar{\mathcal{U}}^{*\beta 1}_{ij}(\mathbf{r}'\sigma')}{\hbar\omega - (E_i + E_j) + i\eta} - \frac{\mathcal{U}^{\alpha 2}_{ij}(\mathbf{r}\sigma)\bar{\mathcal{U}}^{*\beta 2}_{ij}(\mathbf{r}'\sigma')}{\hbar\omega + (E_i + E_j) + i\eta}. \tag{2.26}$$

By definition, the QRPA Green function $\mathbf{G}$ relates the perturbing external field to the density change,

$$\boldsymbol{\rho}' = \mathbf{G}\mathbf{F}. \tag{2.27}$$

Combining with Eq. (2.24) we obtain the generalized Bethe-Salpeter equation,

$$\mathbf{G} = (1 - \mathbf{G}_0\mathbf{V})^{-1}\mathbf{G}_0 = \mathbf{G}_0 + \mathbf{G}_0\mathbf{V}\mathbf{G}. \tag{2.28}$$

In the case of transitions from the ground state to excited states within the same nucleus, only the (ph,ph) component of $\mathbf{G}$ is acting. If the interaction does not depend on spin variables the strength function is thus given by

$$S(\omega) = -\frac{1}{\pi}\mathrm{Im} \int F^{11*}(\mathbf{r})\mathbf{G}^{11}(\mathbf{r}, \mathbf{r}'; \omega)F^{11}(\mathbf{r}')d\mathbf{r}\ d\mathbf{r}'. \tag{2.29}$$

In the equations above we have not introduced explicitly the isospin degree of freedom. This can be done directly on the final equations by doubling the dimension of the matrices in order to distinguish between neutrons and protons.

B. Spherical symmetry

In the case of spherical symmetry each qp state is denoted by the quantum numbers (E, l, j, m), where E is the qp energy and (ljm) are the standard notations for the orbital and total angular momenta. Performing the summation over the projection of the total angular momentum and over the spin variables one gets for the unperturbed Green function (2.26),

$$\mathbf{G}_0^{\alpha\beta}(\mathbf{r}, \mathbf{r}'; \omega) = \sum_{\substack{l_p j_p; l_q j_q \\ LM}} |A^L_{l_p j_p; l_q j_q}|^2 g^{\alpha\beta}_{l_p j_p; l_q j_q}(r, r'; \omega) \times Y_{LM}(\hat{r})Y^*_{LM}(\hat{r}'), \tag{2.30}$$

where the expression for the geometrical coefficients $A^L_{l_p j_p; l_q j_q}$ is

$$A^L_{l_p j_p; l_q j_q} = \sqrt{\frac{2j_p + 1}{8\pi}}[1 + (-)^{l_p + l_q + L}]\left\langle j_p \frac{1}{2} L 0 \middle| j_q \frac{1}{2} \right\rangle. \tag{2.31}$$

This expression holds for a residual interaction without gradient terms. We do not give here the expressions for the case involving gradient terms since in the calculations of Sec. III we use a Landau-Migdal form for the residual interaction.

The radial Green functions $g^{\alpha\beta}_{l_p j_p; l_q j_q}(r, r'; \omega)$ are expressed in terms of the qp energies E_k and the corresponding radial HFB wave functions, i.e., $u_k(r) = u_{l_k, j_k}(E_k, r)$ and $v_k(r) = v_{l_k, j_k}(E_k, r)$. Thus, the radial Green function for a given pair of quantum numbers $(l_q j_q, l_p j_p)$ is given by

$$g^{\alpha\beta}_{l_p j_p; l_q j_q}(r, r'; \omega) = \sum\!\!\!\!\!\!\int_{E_p, E_q} \frac{\mathcal{U}^{\alpha 1}_{pq}(r)\bar{\mathcal{U}}^{\beta 1}_{pq}(r')}{\hbar\omega - (E_p + E_q) + i\eta} - \frac{\mathcal{U}^{\alpha 2}_{pq}(r)\bar{\mathcal{U}}^{\beta 2}_{pq}(r')}{\hbar\omega + (E_p + E_q) + i\eta}, \tag{2.32}$$

where

$$\mathcal{U}_{pq}(r)=\begin{pmatrix} u_p(r)v_q(r) & u_q(r)v_p(r) \\ -u_p(r)u_q(r) & v_p(r)v_q(r) \\ v_p(r)v_q(r) & -u_p(r)u_q(r) \end{pmatrix},$$

$$\overline{\mathcal{U}}_{pq}=\mathcal{U}_{pq}+\mathcal{U}_{qp}. \tag{2.33}$$

In Eq. (2.32) the $\sum\!\!\!\!\!\!\int$ symbol indicates that the summation is taken both over the discrete and the continuum qp states.

The unperturbed Green function expressed by Eq. (2.30) can be used together with an interaction which does not depend on spin variables in order to get the radial QRPA Green function, given by Eq. (2.28).

All the equations should be written in neutron-proton formalism. Thus, each supermatrix ($\mathbf{G}_0$, $\mathbf{G}$, $\mathbf{V}$) is divided in nine blocks corresponding to the ph, pp, hh case and each one of these blocks is divided in four sub-blocks corresponding to the nn, np, pn, and pp quantities. The way to calculate explicitly the residual interaction supermatrix is given in the Appendix.

C. The energy-weighted sum rule in the QRPA

It is often stated that the Thouless theorem [12] concerning the energy-weighted sum rule (EWSR) of RPA is also valid for the QRPA. We give here an explicit proof of this theorem for the nontrivial case of QRPA.

The Thouless theorem extended to the QRPA means that the equality

$$\sum_{\nu} E_{\nu}|\langle \nu|F|\mathrm{QRPA}\rangle|^2=\tfrac{1}{2}\langle \mathrm{HFB}|[F,[H,F]]|\mathrm{HFB}\rangle \tag{2.34}$$

must be satisfied. In the above equation, $|\mathrm{HFB}\rangle$ is the HFB ground state and $|\mathrm{QRPA}\rangle$ is the correlated QRPA ground state while $|\nu\rangle$ stands for the excited QRPA states.

To demonstrate this equality we use the QRPA equations in configuration space [1]. The specific point of the demonstration is that the one-body operator F is now expressed in terms of qp operators,

$$F=\sum_{kk'} f_{kk'}c_k^{\dagger}c_{k'}=\sum_{\substack{kk'\\ll'}} f_{kk'}[U_{kl}^{*}U_{k'l'}\beta_l^{\dagger}\beta_{l'}+U_{kl}^{*}V_{k'l'}\beta_l^{\dagger}\beta_{l'}^{\dagger}$$
$$+V_{kl}^{*}U_{k'l'}\beta_l\beta_{l'}+V_{kl}^{*}V_{k'l'}\beta_l\beta_{l'}^{\dagger}]. \tag{2.35}$$

The calculation of the left-hand side (lhs) of Eq. (2.34) introduces quantities such as $\langle \mathrm{QRPA}|F|\nu\rangle$. They can be written as

$$\langle \mathrm{QRPA}|F|\nu\rangle=(\overline{f}^{T} \quad \overline{f}^{\dagger})\begin{pmatrix} X^{\nu} \\ Y^{\nu} \end{pmatrix}, \tag{2.36}$$

where

$$\overline{f}_{ll'}=\sum_{kk'} f_{kk'}h_{kk'll'}, \tag{2.37}$$

$$h_{kk'll'}=V_{kl'}^{*}U_{k'l}-V_{kl}^{*}U_{k'l'}. \tag{2.38}$$

Equation (2.36) allows us to get for the lhs of Eq. (2.34) an expression similar to the one of Ref. [12] [Eq. (36)], i.e.,

$$S_1=\frac{1}{2}\begin{pmatrix} \overline{f}^{T} & -\overline{f}^{\dagger} \end{pmatrix}\begin{pmatrix} A & B \\ B^{*} & A^{*} \end{pmatrix}\begin{pmatrix} \overline{f}^{*} \\ -\overline{f} \end{pmatrix}. \tag{2.39}$$

The right-hand side (rhs) of Eq. (2.34) is obtained by using Eq. (2.35) and the definition of the A and B matrices of QRPA,

$$A_{kk'll'}=\langle \mathrm{HFB}|[\beta_{k'}\beta_k,[H,\beta_l^{\dagger}\beta_{l'}^{\dagger}]]|\mathrm{HFB}\rangle, \tag{2.40}$$

$$B_{kk'll'}=-\langle \mathrm{HFB}|[\beta_{k'}\beta_k,[H,\beta_{l'}\beta_l]]|\mathrm{HFB}\rangle, \tag{2.41}$$

with $k<k'$ and $l<l'$. Expressing the rhs with A, B, and $\overline{f}$ leads to Eq. (2.39).

This proof is valid for a density-independent force. In the case of a density-dependent force the relation should remain valid provided the density-dependent terms commute with F, as it has been shown for the RPA case [1].

III. HFB+QRPA CALCULATIONS OF OXYGEN ISOTOPES

A. HFB calculations

We apply our formalism to the calculation of neutron-rich oxygen isotopes ^{18,20,22,24}O. The ground states are calculated within the continuum HFB approach [11] where the continuum is treated exactly. The HFB equations are solved in coordinate space with a step of 0.25 fm for the radial coordinate. In the HFB the mean field quantities are calculated by using the Skyrme interaction SLy4 [13], while for the pairing interaction we take a zero-range density-dependent interaction given by

$$V_{pair}=V_0\left[1-\left(\frac{\rho(r)}{\rho_0}\right)^{\alpha}\right]\delta(\mathbf{r_1}-\mathbf{r_2}), \tag{3.1}$$

where V_0, ρ_0, and α are the parameters of the force. Due to its zero range, this force should be used in the HFB calculations with a cutoff in qp energy. To minimize the number of free parameters, we adapt here the prescription of Refs. [14,15] which relates the energy cutoff with the V_0 value for the free neutron-neutron system. To extend this prescription to finite nuclei, we use the relation between the energy ε of the particle inside nucleus and the energy ε_0 of a free particle,

$$\varepsilon(k)=\varepsilon^{0}(k)\frac{m}{m^{*}}+U_{HF}, \tag{3.2}$$

where m^{*} is the effective mass, k the momentum, and U_{HF} the Hartree-Fock potential. Since m^{*} depends on the density we take $m^{*}/m=0.7$, which is the bulk value for m^{*}. From ϵ_{cutoff} we can deduce the qp cutoff energy E_{cutoff}. With this prescription we verified that the calculated HFB neutron

TABLE I. Neutron pairing gaps, Δ_{Exp} is the experimental value taken as the odd-even mass difference [16], Δ_{Phen} is using the empirical $12/\sqrt{A}$ MeV prescription [17], Δ_{HFB} is calculated in the present work, and Δ_{WS} is the gap used in Ref. [10].

	Δ_{Exp} (MeV)	Δ_{Phen} (MeV)	Δ_{HFB} (MeV)	Δ_{WS} (MeV)
^{18}O	1.95	2.83	1.96	2.74
^{20}O	1.83	2.68	1.85	3.13
^{22}O	1.52	2.56	1.04	3.30
^{24}O	0.49	2.45	0.00	3.39

pairing gap Δ_n remains constant for each couple (V_0, E_{cutoff}). In the HFB calculations we choose a qp cutoff energy equal to 50 MeV. Then, the prescription of Ref. [14] gives $V_0 = -415.73$ MeV fm^3. The parameter ρ_0 is set to the usual saturation density, 0.16 fm^{-3}. The value of the parameter α is chosen so as to reproduce the trend of the experimental gap. Note that the calculated gap is defined as the integral of the pairing field whereas the experimental gap is related to mass differences of the neighboring nuclei and therefore, there is no need to have an exact quantitative agreement. We find that the best choice is $\alpha = 1.5$. Note that the trend of the experimental gap is at variance with the empirical rule $\Delta = 12/\sqrt{A}$ MeV. All the pairing gap values are displayed in Table I. It should be noted that, in the case of HFB+Skyrme calculations, if one has a reasonable pairing gap in ^{18,20}O then the pairing is weaker in ^{22}O and absent in ^{24}O. This is due to the $1d_{5/2}$ and $2s_{1/2}$ subshell closure. A similar trend is observed in calculations using Gogny interaction [18]. As seen in Table I, in the case of QRPA calculations using a Woods-Saxon potential [10] the gaps are larger due to the fact that the energy distance between the relevant subshells is smaller.

B. QRPA calculations

In the QRPA calculations the residual interaction is derived in principle from the interaction used in the HFB, i.e., the Skyrme force and the pairing force (3.1). The zero-range part of the forces pose no problem. The velocity-dependent terms of the Skyrme force bring additional complications which can be avoided by approximating the residual interaction in the (ph,ph) subspace by its Landau-Migdal limit [19] where the interacting particle and hole have the Fermi momentum and the transferred momentum is zero. The Skyrme interaction has only $l=0$ and $l=1$ Landau parameters. Taking the Landau-Migdal form for the (ph,ph) interaction simplifies greatly the numerical task, at the cost of the loss of some consistency. In this work we calculate only natural parity (non-spin-flip) excitations and we drop the spin-spin part of the (ph,ph) interaction which plays a minor role. The Coulomb and spin-orbit residual interactions are also dropped.

The QRPA Green function can be evaluated starting with the unperturbed Green function given by Eq. (2.32). The latter is constructed by using the solutions of the HFB equations, i.e., the qp energies and the corresponding wave functions U and V. All the qp states are included until an energy cutoff of 50 MeV, allowing pairs of qp energy until 100 MeV. In a schematic picture, these pairs are representative of excitations from the ^{16}O core, and also excitations of the valence neutrons. The generalized Bethe-Salpeter equation (2.28) is solved with a step of 0.5 fm and all radial integrals are carried out up to 22.5 fm. The strength distribution is calculated until $\omega_{Max} = 50$ MeV, with a step of 100 keV and an averaging width $\eta = 150$ keV. We have studied two variants of calculations, the full continuum variant and a box variant where the qp spectrum is discretized by calculating the HFB solutions with a box boundary condition, the box radius being 22.5 fm. For ^{24}O only box calculations have been performed.

In a fully consistent calculation the spurious center-of-mass state should come out at zero energy. Because of the Landau-Migdal form of the interaction adopted here the consistency between mean field and residual qp interaction is broken and the spurious state becomes imaginary. We cure this defect by renormalizing the residual interaction by a factor α. We find that in all cases the spurious state $J^\pi = 1^-$ comes out at zero energy for $\alpha = 0.80$. We have checked that the EWSR are satisfied within 1% to 5%.

C. Quadrupole excitations in oxygen isotopes

We calculate quadrupole strength distributions with the operators $F_0 = \Sigma_i r_i^2 Y_{20}(\hat{r}_i)$ (isoscalar) and $F_0 = \Sigma_i r_i^2 Y_{20}(\hat{r}_i) t_z(i)$ (isovector). All results presented correspond to the SLy4 interaction except when stated otherwise. The strength distributions calculated in the neutron-rich oxygen isotopes are displayed in Fig. 1.

One can identify a strong low-lying state and the giant quadrupole resonance (GQR). The low-lying state becomes more isospin admixed as the neutron excess increases. In the case of ^{24}O the strength distribution is similar to that calculated in Ref. [10] with a Woods-Saxon potential for the mean field, although pairing effects are negligible in our calculation whereas the gap Δ of Ref. [10] is sizable. The main difference is the position of the first 2^+ state located at 4.0 MeV here and 5.0 MeV in Ref. [10]. In the other nuclei this low-lying state is at lower energies. This is due to the $2s_{1/2}$ subshell closure in ^{24}O. The HF single-particle energies are given in Table II. The $2s_{1/2}$ state is more bound in the ^{24}O nucleus, suggesting a stronger subshell closure in this case. The occupation factors of these states calculated in HFB are displayed in Table II. The $2s_{1/2}$ starts to be significantly populated in ^{22}O due to the pairing correlations. In the ^{18,20}O spectra mainly three low-lying peaks are present. In the unperturbed case they correspond to the $(1d_{5/2},1d_{5/2})$, $(1d_{5/2},2s_{1/2})$, and $(1d_{5/2},1d_{3/2})$ two-qp neutron configurations. Their energies are given in Table III. In ^{18,20}O the configuration $(1d_{5/2},1d_{3/2})$ has a very low strength whereas the $(1d_{5/2},1d_{5/2})$, $(1d_{5/2},2s_{1/2})$ configurations have similar strength. The effect of the residual interaction, in addition to admix the configurations, is to lower the energy of the initial $(1d_{5/2},1d_{5/2})$ peak and to increase the strength of the low-lying state (cf. Fig. 1).

The effect of the residual interaction in ^{22}O is displayed in Fig. 2, showing the isoscalar strength functions calculated with the unperturbed Green function G_0 and with the full G.

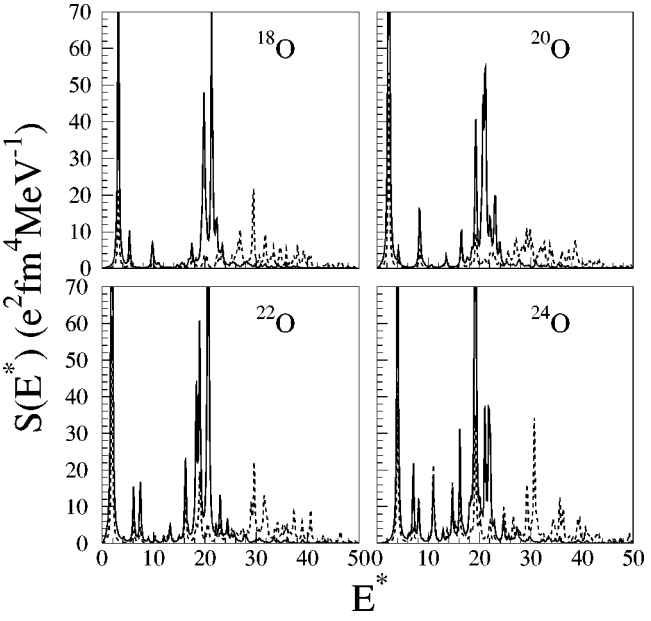

FIG. 1. Isoscalar (solid line) and isovector (dashed line) quadrupole strength functions calculated in continuum QRPA for the ^{18,20,22,24}O isotopes.

The effect of the residual interaction is to gather the strength to generate collective modes such as the GQR and the low-lying state.

The $E2$ energy and $B(E2)$ value of the first 2^+ state are displayed in Table IV. As noted before, the $E2$ energy in ^{24}O is larger than in other isotopes due to the $2s_{1/2}$ subshell closure. The $E2$ energy in ^{18}O is overestimated and that of ^{22}O is underestimated as compared to experiment. This shows, as noted previously in QRPA calculations with a constant gap (Ref. [24]), that the energy prediction of the low-lying modes is a delicate task in RPA-type models. The $B(E2)$ values are well reproduced except for the problematic ^{18}O nucleus. This discrepancy observed for the $B(E2)$ value of ^{18}O is also found in several shell-model calculations [25,26] and in previous QRPA calculations [24], showing a limitation of such models to study ^{18}O low-lying states. Indeed this high $B(E2)$ anomaly may be due to the presence of deformed states in the experimental low-lying spectra of ^{18}O [27]. Moreover, the observation of many low-lying states in this nucleus can be described by bands characteristics of the rotational spectra. It has been suggested that the low-lying states in these nuclei (such as ^{16,17,18}O) can be described as a mixture between highly deformed states and the usual shell model states [27,28]. This allows to successfully reproduce both the $E2$ and $B(E2)$ of the low-lying states. As stated in Ref. [27], for heavier oxygen isotopes, the energies of the deformed states become higher, and thus the admixture is smaller. This may explain why the calculated $B(E2)$ are in good agreement with the experimental data for ^{20,22}O nuclei. The $B(E2)$ in ^{24}O is predicted smaller than those of lighter isotopes, which supports the $2s_{1/2}$ subshell closure effect. In order to display the structure of the low-lying sector, the calculated energies and $B(E2)$ of the second and third 2^+ states are shown in Table V for the oxygen isotopes. The 2_2^+ and 2_3^+ energies are overestimated in the case of ^{18}O, whereas a good agreement is found for the energy of the 2_2^+ state for ^{20}O. This may support the presence of deformed admixtures in the light neutron-rich oxygen isotopes such as ^{18}O.

The calculated M_n/M_p ratios indicate that the neutron are more coherently contributing to the excitation when their number is increasing. For example, the M_n/M_p ratio for ^{24}O is more than twice the N/Z value, indicating a very strong neutron contribution to the excitation. The calculated M_n/M_p ratio is correctly reproducing that of ^{20}O deduced from proton scattering experiments. In the case of ^{18}O the experimental M_n/M_p is not well reproduced. This is linked to the fact that the $B(E2)$ value is not well described by the model. The transition densities for the first low-lying 2^+

TABLE II. $1d_{5/2}$, $2s_{1/2}$, and $1d_{3/2}$ levels in the ^{18,20,22,24}O nuclei. For each nucleus the left column shows the single-particle energies (MeV) calculated with the HF approximation, and the right column displays the occupation factors for the single-qp levels calculated with the HFB model.

	^{18}O		^{20}O		^{22}O		^{24}O	
$1d_{5/2}$	-6.7	0.31	-6.9	0.62	-7.2	0.93	-7.7	1
$2s_{1/2}$	-4.0	0.03	-4.2	0.08	-4.6	0.18	-4.9	1
$1d_{3/2}$	0.3	0.01	0.3	0.02	0.2	0.01	0.2	0

TABLE III. Two qp energies (MeV) of the $(1d_{5/2},1d_{5/2})$, $(1d_{5/2},2s_{1/2})$, and $(1d_{5/2},1d_{3/2})$ configurations of the unperturbed strength function for the ^{18,20,22}O nuclei.

	^{18}O	^{20}O	^{22}O
$(1d_{5/2},1d_{5/2})$	4.52	4.16	4.60
$(1d_{5/2},2s_{1/2})$	5.72	4.36	3.35
$(1d_{5/2},1d_{3/2})$	10.39	9.09	7.70

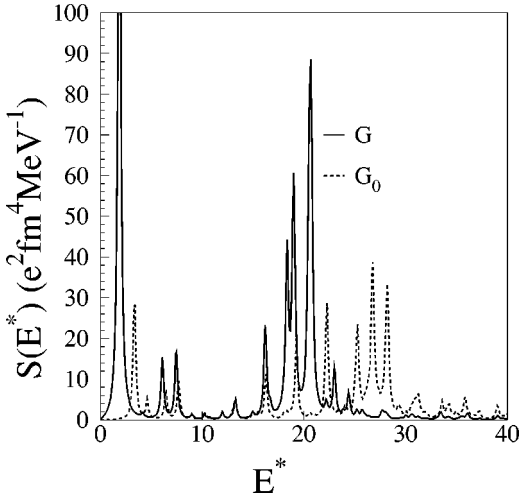

FIG. 2. Isoscalar quadrupole strength function calculated in continuum QRPA for the ^{22}O nucleus. The unperturbed strength (dashed line) is also shown.

TABLE IV. Energy, proton contribution to the reduced transition probabilities $B(E2)$, and ratio of the transition matrix elements M_n/M_p for the first 2^+ state in the ^{18,20,22,24}O nuclei, calculated with the present model. Measured $E2$, $B(E2)$ values and the M_n/M_p ratios corresponding to the experimental data are displayed in brackets.

	^{18}O	^{20}O	^{22}O	^{24}O
$E2$ (MeV)	3.2/(2.0) [a]	2.3/(1.7) [a]	1.9/(3.2) [b]	4.0
$B(E2)$ (e^2fm^4)	14/(45±2) [c]	22/(28±2) [c]	22/(21±8) [d]	9
$(M_n/M_p)_{2^+}$	2.88/(1.10±0.24) [e]	3.36/(3.25±0.80) [e]	3.53	4.37

[a]Reference [20].
[b]Reference [21].
[c]Reference [22].
[d]Reference [23].
[e]Reference [24].

state of the neutron-rich oxygen isotopes are displayed in Fig. 3. In the case of ^{22,24}O the neutron transition density is located more on the surface than the proton one, possibly indicating the presence of a neutron skin.

The pairing effects are depicted in Fig. 4, where the continuum QRPA calculation is compared to a HF+RPA calculation for the ^{22}O nucleus. The effect of pairing is to shift to higher energy the low-lying peak, and to split the second 2^+ state into two states with smaller strength. There is also some effect in the GQR region.

In order to investigate the effect of the density dependence of the pairing interaction we have also calculated the strength distributions with a density-independent interaction, i.e., ρ_0 going to infinity in Eq. (3.1). In the HFB calculation, the V_0 parameter has been chosen to reproduce the experimental gap of ^{18}O, $V_0 = -220$ MeV fm^3 (in this case the prescription of Ref. [14] is no longer applied). Figure 5 compares the results in ^{18}O calculated with the density-dependent and density-independent interactions. The effect of the density dependence is to increase the energies of the 2^+ states, and to slightly lower the strength of the low-lying states.

Box discretization calculations have also been performed in order to test the box boundary condition approximation. The results are shown in Fig. 6 for ^{22}O. One can see that only the low-lying state is nearly insensitive whereas the structure of the GQR is more affected by the way the continuum is treated. This shows the necessity of the exact continuum treatment in order to study the giant resonances in neutron-rich oxygen isotopes.

TABLE V. Energy and proton contribution to the reduced transition probabilities $B(E2)$ in the ^{18,20,22,24}O nuclei, calculated with the present model for the 2_2^+ (upper lines) and 2_3^+ (lower lines) states. Measured $E2$ values corresponding to the experimental data are displayed in brackets.

	^{18}O	^{20}O	^{22}O	^{24}O
2_2^+ : $E2$ (MeV)	5.3/(4.0) [a]	4.2/(4.1) [a]	6.2	7.1
2_2^+ : $B(E2)$ (e^2fm^4)	1.0	0.3	1.4	4.0
2_3^+ : $E2$ (MeV)	9.8/(5.3) [a]	8.3/(5.2) [a]	7.5	8.1
2_3^+ : $B(E2)$ (e^2fm^4)	1.5	2.5	2.5	0.7

[a]Reference [20].

Since our full calculations (HFB+QRPA) have only the Skyrme and the pairing interaction as inputs, the results may be used to learn about the different Skyrme parametrizations. Figure 7 shows a comparison of results obtained with the SLy4 [13], SGII [7], and SIII [29] for the ^{20}O nucleus. There is no drastic effect depending on the force. The SIII interaction shifts some low-lying states to higher energy and increases the strength of the state located around 5 MeV. All three interactions produce a splitting of the GQR but the SGII force predicts more strength in the lower component of the giant resonance.

IV. CONCLUSIONS

We have derived the Bethe-Salpeter equation for the QRPA from the small amplitude limit of the perturbed time dependent HFB equations. This approach ensures the self-consistency at the conceptual level between the mean field, the pairing field, and the qp residual interaction. The QRPA

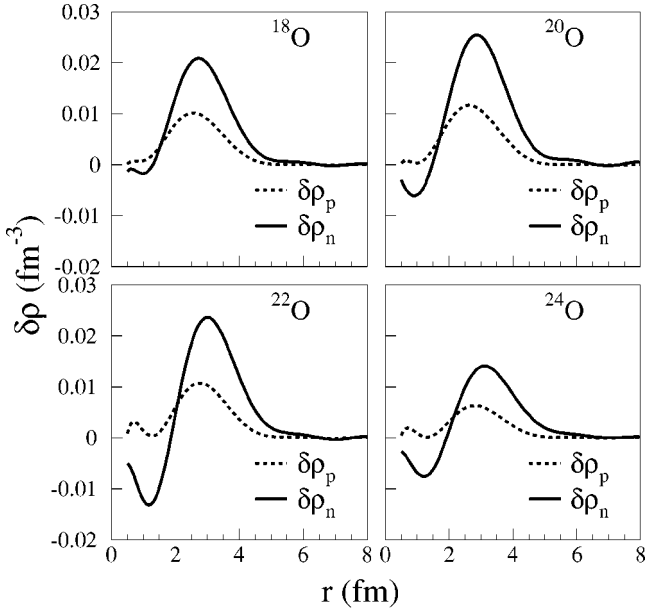

FIG. 3. Neutron and proton transition densities of the first 2^+ state of ^{18,20,22,24}O nuclei.

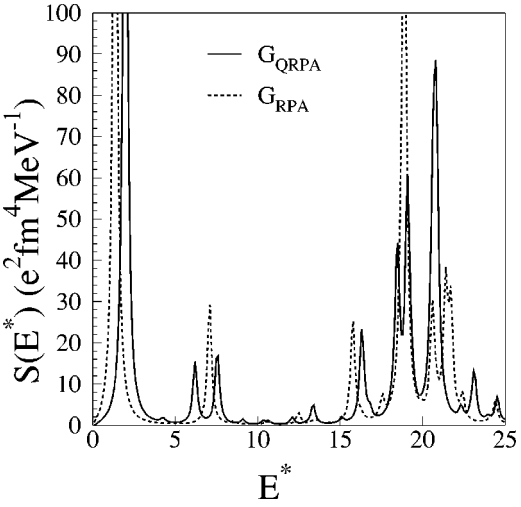

FIG. 4. Isoscalar strength function calculated in continuum QRPA (solid line) and HF+RPA (dashed line) with box boundary conditions for the ^{22}O nucleus.

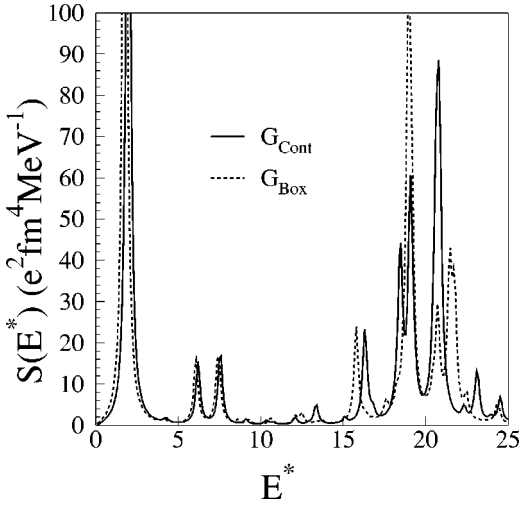

FIG. 6. Isoscalar strength function calculated in continuum QRPA (solid line) and with a box discretization (dashed line) for the ^{22}O nucleus.

Green function is decomposed into the ph, pp, and hh channels. The supermatrix representing the residual interaction is determined self-consistently from the Skyrme and the pairing interactions used in the HFB calculations. The Thouless theorem concerning the EWSR sum rule is shown to hold in the case of self-consistent QRPA.

As an application we have studied the quadrupole excitations of the neutron-rich oxygen isotopes using Skyrme-type interactions for the mean field and a zero-range, density-dependent interaction for the pairing field. In the numerical study we have approximated the ph residual interaction coming from the Skyrme force by its Landau limit. The coupling to the continuum appears to have a sizable effect on the GQR and a minor effect on the low-lying states. This shows the importance of the full continuum treatment in order to study giant resonances in neutron-rich nuclei. The low-lying states are sensitive to the pairing interaction. The first 2^+ state of ^{18}O is not well described, as previously noted with other models such as shell-model calculations. Additional investigations on this nucleus are called for. The continuum QRPA shows its ability to reproduce the experimental data of the first 2^+ state for heavier oxygen isotopes, and it predicts a lowering of the $B(E2)$ value for the ^{24}O nucleus. A future improvement of the model will be to include fully the velocity-dependent terms of the Skyrme interaction in the ph channel. Work along these lines is in progress.

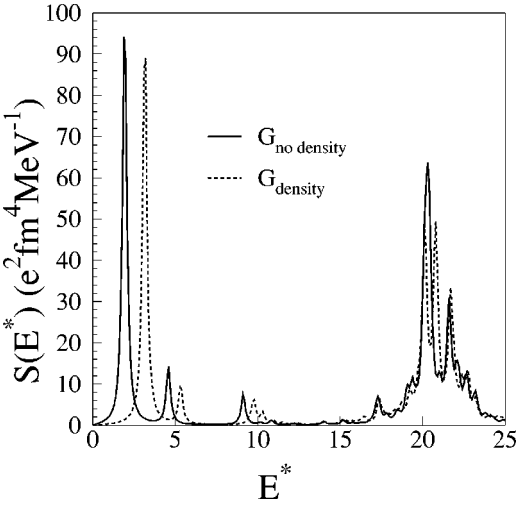

FIG. 5. Isoscalar strength function calculated with a density-independent pairing interaction (solid line) and density-dependent pairing interaction (dashed line) with box boundary conditions for the ^{18}O nucleus.

APPENDIX A: HAMILTONIAN PERTURBATION AND RESIDUAL INTERACTION

The HFB energy functional is written as follows:

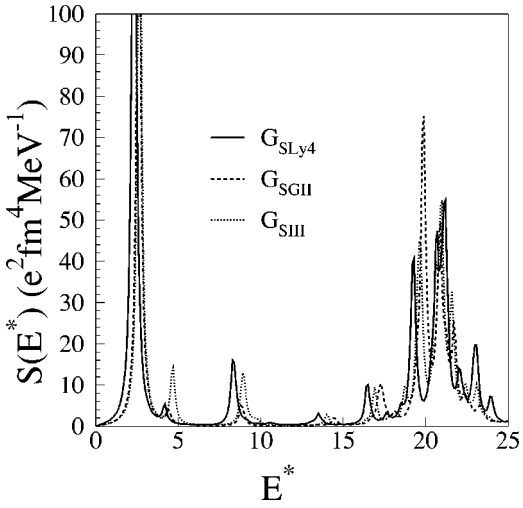

FIG. 7. Isoscalar quadrupole strength function calculated in continuum QRPA for the ^{20}O nucleus with various Skyrme interactions: SLy4 (solid line), SGII (dashed line), and SIII (dotted line).

$$\mathcal{E}=\sum_{ml} t_{ml}\rho_{ml}+\frac{1}{2}\sum_{mlpq}\langle lq|\bar{\mathcal{V}}|mp\rangle\rho_{pq}\rho_{ml}$$

$$+\frac{1}{4}\sum_{mlpq}\langle lm|\bar{\mathcal{V}}_P|pq\rangle\kappa^*_{lm}\kappa_{pq}, \tag{A1}$$

with $\bar{\mathcal{V}}$ the antisymmetrized interaction and $\bar{\mathcal{V}}_p$ the antisymmetrized pairing interaction.

The HFB Hamiltonian is

$$\mathcal{H}^0_{ij}=\begin{pmatrix} h_{ij} & \Delta_{ij} \\ \Delta^\dagger_{ij} & -h^*_{ji}\end{pmatrix} \tag{A2}$$

with

$$h_{ij}=\frac{\partial\mathcal{E}}{\partial\rho_{ij}},\Delta_{ij}=\frac{\partial\mathcal{E}}{\partial\kappa^*_{ij}}. \tag{A3}$$

Next we expand the perturbation of the Hamiltonian on the densities perturbations and get

$$\mathcal{H}'^{11}_{ij}=\sum_{kl}\frac{\partial^2\mathcal{E}}{\partial\rho_{kl}\partial\rho^*_{ij}}\rho'_{kl}+\frac{1}{2}\frac{\partial^2\mathcal{E}}{\partial\kappa_{kl}\partial\rho^*_{ij}}\kappa'_{kl}+\frac{1}{2}\frac{\partial^2\mathcal{E}}{\partial\bar{\kappa}_{kl}\partial\rho^*_{ij}}\bar{\kappa}_{kl}, \tag{A4}$$

$$\mathcal{H}'^{12}_{ij}=\sum_{kl}\frac{\partial^2\mathcal{E}}{\partial\rho_{kl}\partial\kappa^*_{ij}}\rho'_{kl}+\frac{1}{2}\frac{\partial^2\mathcal{E}}{\partial\kappa_{kl}\partial\kappa^*_{ij}}\kappa'_{kl}, \tag{A5}$$

$$\mathcal{H}'^{21}_{ij}=\sum_{kl}\frac{\partial^2\mathcal{E}}{\partial\rho_{kl}\partial\bar{\kappa}^*_{ij}}\rho'_{kl}+\frac{1}{2}\frac{\partial^2\mathcal{E}}{\partial\bar{\kappa}_{kl}\partial\bar{\kappa}^*_{ij}}\bar{\kappa}'_{kl}, \tag{A6}$$

$$\mathcal{H}'^{22}_{ij}=-\mathcal{H}'^{11}_{ji}. \tag{A7}$$

To get $\mathcal{H}'$ in coordinate space, we use the relationship between the densities,

$$\rho(\mathbf{r}\sigma)=\sum_{ij}\phi^*_i(\mathbf{r}\sigma)\phi_j(\mathbf{r}\sigma)\rho_{ji}, \tag{A8}$$

$$\kappa(\mathbf{r}\sigma)=\sum_{ij}\phi_i(\mathbf{r}\bar{\sigma})\phi_j(\mathbf{r}\sigma)\kappa_{ji}, \tag{A9}$$

$$\bar{\kappa}(\mathbf{r}\sigma)=\sum_{ij}\phi^*_i(\mathbf{r}\bar{\sigma})\phi^*_j(\mathbf{r}\sigma)\kappa^*_{ji}, \tag{A10}$$

where $\phi_i(\mathbf{r}\sigma)$ is the nucleon wave function.

Using Eqs. (A4)–(A7) together with Eqs. (A8)–(A10) allows to calculate $\mathcal{H}'$ in coordinate space, and get Eq. (2.22).

[1] P. Ring and P. Schuck, *The Nuclear Many-Body Problem* (Springer-Verlag, Berlin, 1980).
[2] R. Arvieu and M. Vénéroni, C. R. Acad. Sci. III **250**, 992 (1960).
[3] M. Kobayasi and T. Marumori, Prog. Theor. Phys. **23**, 387 (1960).
[4] M. Baranger, Phys. Rev. **120**, 957 (1960).
[5] G. F. Bertsch and S. F. Tsai, Phys. Rep. **18**, 125 (1975).
[6] K. F. Liu and Nguyen Van Giai, Phys. Lett. **65B**, 23 (1976).
[7] Nguyen Van Giai and H. Sagawa, Nucl. Phys. **A371**, 1 (1981).
[8] S. Kamerdzhiev, R. J. Liotta, E. Litvinova, and V. Tselyaev, Phys. Rev. C **58**, 172 (1998).
[9] K. Hagino and H. Sagawa, Nucl. Phys. **A695**, 82 (2001).
[10] M. Matsuo, Nucl. Phys. **A696**, 371 (2001).
[11] M. Grasso, N. Sandulescu, Nguyen Van Giai, and R. J. Liotta, Phys. Rev. C **64**, 064321 (2001).
[12] D. J. Thouless, Nucl. Phys. **22**, 78 (1961).
[13] E. Chabanat, P. Bonche, P. Haensel, J. Meyer, and R. Schaeffer, Nucl. Phys. **A635**, 231 (1998).
[14] E. Garrido, P. Sarriguren, E. Moya de Guerra, and P. Schuck, Phys. Rev. C **60**, 064312 (1999).
[15] G. F. Bertsch and H. Esbensen, Ann. Phys. (N.Y.) **209**, 327 (1991).
[16] G. Audi and A. H. Wapstra, Nucl. Phys. **A595**, 409 (1995).
[17] A. Bohr and B. Mottelson, *Nuclear Structure* (Benjamin, New York, 1969), Vol. 1, p. 169.
[18] J. Libert (private communication).
[19] S. O. Bäckman, A. D. Jackson, and J. Speth, Phys. Lett. **56B**, 209 (1975).
[20] R. B. Firestone, *Table of Isotopes*, 8th ed. (Wiley-Interscience, New York, 1996).
[21] M. Belleguic, M. J. Lopez-Jimenez, M. Stanoiu, F. Azaiez, M.-G. Saint-Laurent, O. Sorlin, N. L. Achouri, J.-C. Angelique, C. Bourgeois, C. Borcea, J.-M. Daugas, C. Donzaud, F. De Oliveira-Santos, J. Duprat, S. Grevy, D. Guillemaud-Mueller, S. Leenhardt, M. Lewitowicz, Yu.-E. Penionzhkevich, and Yu. Sobolev, Nucl. Phys. **A682**, 136c (2001).
[22] S. Raman, C. H. Malarkey, W. T. Milner, C. W. Nestor, Jr., and P. H. Stelson, At. Data Nucl. Data Tables **36**, 1 (1987).
[23] P. G. Thirolf, B. V. Pritychenko, B. A. Brown, P. D. Cottle, M. Chromik, T. Glasmacher, G. Hackman, R. W. Ibbotson, K. W. Kemper, T. Otsuka, L. A. Riley, and H. Scheit, Phys. Lett. B **485**, 16 (2000).
[24] E. Khan, Y. Blumenfeld, Nguyen Van Giai, T. Suomijarvi, N. Alamanos, F. Auger, G. Colo, N. Frascaria, A. Gillibert, T. Glasmacher, M. Godwin, K. W. Kemper, V. Lapoux, I. Lhenry, F. Marechal, D. J. Morrissey, A. Musumarra, N. A. Orr, S. Ottini-Hustache, P. Piattelli, E. C. Pollacco, P. Roussel-Chomaz, J. C. Roynette, D. Santonocito, J. E. Sauvestre, J. A. Scarpaci, and C. Volpe, Phys. Lett. B **490**, 45 (2000).
[25] B. A. Brown and B. H. Wildenthal, Annu. Rev. Nucl. Part. Sci. **38**, 29 (1988).
[26] Y. Utsuno, T. Otsuka, T. Mizusaki, and M. Honma, Phys. Rev. C **60**, 054315 (1999).
[27] G. E. Brown and A. M. Green, Nucl. Phys. **75**, 401 (1966).
[28] P. Federman and I. Talmi, Phys. Lett. **15**, 165 (1965).
[29] M. Beiner, H. Flocard, Nguyen Van Giai, and P. Quentin, Nucl. Phys. **A238**, 29 (1975).